A Novel Structure for Single-Switch Nonisolated Transformerless Buck–Boost DC–DC Converter

Mohammad Reza Banaei and Hossein Ajdar Faeghi Bonab

***Abstract*—A novel transformerless buck–boost dc–dc converter is proposed in this paper. The presented converter voltage gain is higher than that of the conventional boost, buck–boost, CUK, SEPIC, and ZETA converters, and high voltage can be obtained with a suitable duty cycle. In this converter, only one power switch is utilized. The voltage stress across the power switch is low. Hence, the low on-state resistance of the power switch can be selected to decrease conduction loss of the switch and improve efficiency. The presented converter has simple structure, therefore, the control of the proposed converter will be easy. The principle of operation and the mathematical analyses of the proposed converter are explained. The validity of the presented converter is verified by the experimental results.**

***Index Terms*—Power switch, transformerless buck–boost dc–dc converter, voltage gain, voltage stress.**

I. Introduction

In recent years, environmental troubles, such as climate change and global warming by increased emissions of carbon dioxide, are very important. With increasing attention to environmental problems, energy achieved from the fuel cell systems is focused on the low environmental effects and clean energy. Fuel cells are an effective alternative to replace fuels in emergency power systems and vehicles. User can use fuel cells as clean energy with low emissions of carbon dioxide. Due to steady operation with renewable fuel supply and high effectiveness and efficiency, the fuel cell has been recognized increasingly as a suitable alternative source. There are some problems of this fuel, such as high costs, but they have brilliant features, such as high efficiency and small size. Due to this explanation, the fuel cell is appropriate as power supplies for telecom back-up facilities and hybrid electric vehicles. The output voltage of the fuel cell unit cell is low and is not steady and it cannot be directly connected to the load. For applications that need a steady dc voltage, buck–boost dc–dc converter is required [1]–[5]. However, the traditional buck–boost converter is not suitable for fuel cells sources. The traditional buck–boost converter efficiency is expected to be high, however, it is low and is limited by the effects of diodes, switches, and equivalent series resistance (ESR) of capacitors and inductors [6]. In order to obtain the high efficiency and high voltage gain, many high step-up dc–dc converters have been proposed and in order to use the low duty cycle, adding a new control method is a good choice [7], [8]. For example, the high step-up voltage gain can be achieved by using a flyback converter with low duty cycle. The voltage gain of the flyback converter can be increased by raising the turns ratio of the transformer. Although the flyback converter can obtain the high step-up voltage gain, the power switches suffer a voltage spike across the switches and the converter efficiency is not high because of the reverse-recovery problems and leakage inductor [9]–[11]. In [12] and [13], high voltage gain dc–dc converters with a coupled inductor are proposed. The leakage inductance of the coupled inductor is so important that it causes high voltage spikes and adds the voltage stress. In [14], the switched capacitor method is used to obtain high step-up voltage gain. In [15], a high step-up bidirectional dc–dc converter with low voltage stress on the switch is proposed. In [16], a high conversion ratio bidirectional dc–dc converter is proposed. However, this converter has five power switches that increase the conduction losses and the cost of the circuit and decrease the efficiency. In [17], a transformerless interleaved high step-down converter is proposed, but, in the presented converter, two power switches have been utilized and the capacitors of the converter are suddenly charged. In [18], transformerless high step-up dc–dc converters are proposed. In [19], a transformerless buck–boost dc–dc converter is proposed. The voltage gain for this converter is twice as large as that of the conventional buck–boost converter. In [20], a buck–boost converter based on KY converter is proposed. In this converter, two main switches are used and the voltage gain of the presented converter is 2D. In [21], a transformerless buck–boost dc–dc converter based on CUK converter is proposed. The voltage transfer gain for the presented converter is twice as large as that of the conventional buck–boost converter. In [22], a multioutput buck–boost dc–dc converter is proposed. This converter has several output voltages, but, in the presented converter, many power switches have been used. In [23], a two-stage inverting buck–boost converter is proposed. The presented converter is constructed of two parallel conventional buck–boost converters. In [24], a two-stage buck–boost converter for power factor correction is presented and this converter does not require additional power switch. In this paper, a novel single-switch transformerless buck–boost dc–dc converter with high step-up voltage gain and low voltage stress on the power switch is proposed. The voltage transfer gain of the proposed converter is higher than that of the classic buck–boost converter, SEPIC, CUK, and ZETA converters. The structure of the proposed converter is simple, hence the control of the converter will be easy. In this converter, only one main switch is used. The voltage stress across the power switch and

Manuscript received January 27, 2016; revised April 4, 2016 and May 13, 2016; accepted June 2, 2016. Date of publication September 12, 2016; date of current version December 9, 2016.

The authors are with the Department of Electrical Engineering, Azarbaijan Shahid Madani University, Tabriz 5375171379, Iran (e-mail: m.banaei@azaruniv.ac.ir; h.ajdarfaeghi@azaruniv.edu).

Color versions of one or more of the figures in this paper are available online at http://ieeexplore.ieee.org.

Digital Object Identifier 10.1109/TIE.2016.2608321

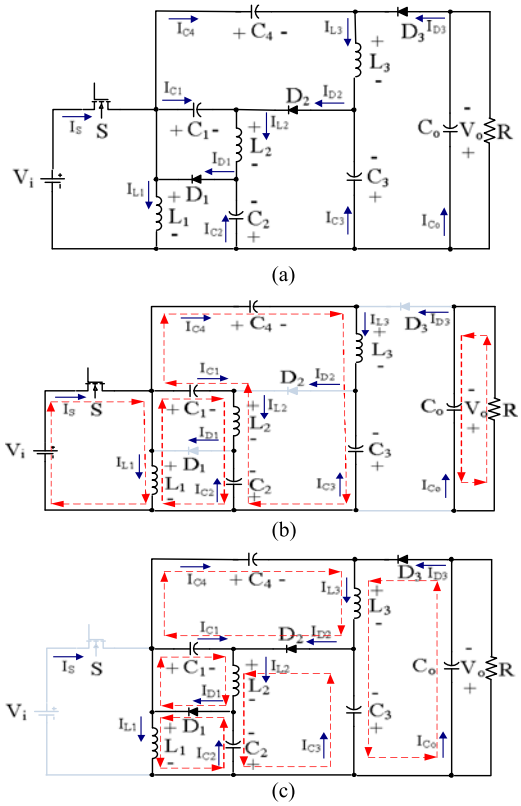

Fig. 1. (a) Equivalent circuit of the proposed converter. (b) Mode 1. (c) Mode 2.

diodes is less than the output voltage, hence the conduction loss of the power switch is low and the efficiency of the presented converter can be improved. The presented converter operates as a universal power supply and it is appropriate for low-voltage and low-power applications and the proposed converter input current is discontinues. The proposed buck–boost converter is utilized in many applications, like fuel-cell systems, car electronic devices, LED drivers, and gadgets, such as mobile phones and notebooks. In this paper, the mathematical analyses of the proposed converter are explained. Besides, to verify the feasibility of the converter, experimental results are provided.

II. Operating Principle of the Proposed Converter

The proposed converter is shown in Fig. 1(a). This converter consists one power switch S, three diodes D_1, D_2, and D_3, three inductors L_1, L_2, and L_3, five capacitors C_1, C_2, C_3, C_4, and C_o and load R.

For simplicity of the analysis of the operating principles, the following assumptions are considered.

1) The capacitors of the presented converter are large enough, hence the voltage across capacitors are assumed to be constant.
2) The main switch of the proposed converter is treated as ideal and the parasitic capacitor of the main switch is neglected.

The presented converter can be operated in both the continuous conduction mode (CCM) and the discontinuous conduction mode (DCM). The CCM can be divided into two operation modes. The analysis of the presented converter in one switching period under CCM is explained in detail as follows:

1) First mode $[0 \le t \le DT_s]$: During this time interval as shown in Fig. 1(b), the switch S is turned ON and the diodes D_1, D_2, and D_3 are turned OFF. The inductors L_1, L_2, and L_3 are magnetized linearly. The capacitors C_1 and C_4 are charged by the capacitors C_2 and C_3. Thus, the relevant equations can be expressed as follows:

$$V_{L1} = V_i \tag{1}$$

$$V_{L2} = V_{C2} - V_{C1} + V_i \tag{2}$$

$$V_{L3} = V_{C3} - V_{C4} + V_i. \tag{3}$$

2) Second mode $[DT_s \le t \le T_s]$: The equivalent circuit is shown in Fig. 1(c). During this time interval, the switch S is turned off and the diodes D_1, D_2, and D_3 are turned on. The inductors L_1, L_2, and L_3 are demagnetized linearly. The capacitor C_2 is charged by the inductor L_1 and the capacitor C_3 is charged by the inductors L_1 and L_2 and the capacitors C_1 and C_4 are discharged. The corresponding equations can be written as follows:

$$V_{L1} = -V_{C2} \tag{4}$$

$$V_{L2} = -V_{C1} = V_{C2} - V_{C3} \tag{5}$$

$$V_{L3} = V_{C1} - V_{C4} = V_{C3} - V_o. \tag{6}$$

III. Steady State Analysis of the Proposed Converter

A. Voltage Gain

By applying volt-sec balance principle on the inductors L_1, L_2, and L_3 and using (1)–(6), we have

$$\frac{1}{T_s}\left(\int_0^{\mathrm{DT}_s} V_i dt + \int_{\mathrm{DT}_s}^{T_s} (-V_{C2}) dt\right) = 0 \tag{7}$$

$$\frac{1}{T_s}\left(\int_0^{\mathrm{DT}_s} (V_{C2} - V_{C1} + V_i) dt + \int_{\mathrm{DT}_s}^{T_s} (-V_{C1}) dt\right) = 0 \tag{8}$$

$$\frac{1}{T_s}\left(\int_0^{\mathrm{DT}_s} (V_{C3} - V_{C4} + V_i) dt + \int_{\mathrm{DT}_s}^{T_s} (V_{C1} - V_{C4}) dt\right) = 0. \tag{9}$$

By using (5) and (7)–(9), the voltage across capacitors C_1, C_2, C_3, and C_4 (V_{C1}, V_{C2}, V_{C3}, and V_{C4}) can be achieved as follows:

$$V_{C1} = V_{C4} = \frac{2DV_i}{1-D} \tag{10}$$

$$V_{C2} = V_{C3} = \frac{DV_i}{1-D}. \tag{11}$$

Using (10) and (11), the voltage transfer gain (M_{CCM}) can be found as follows:

$$M_{\mathrm{CCM}} = \frac{V_o}{V_i} = \frac{V_{C3} + V_{C4}}{V_i} = \frac{3D}{1-D}. \tag{12}$$

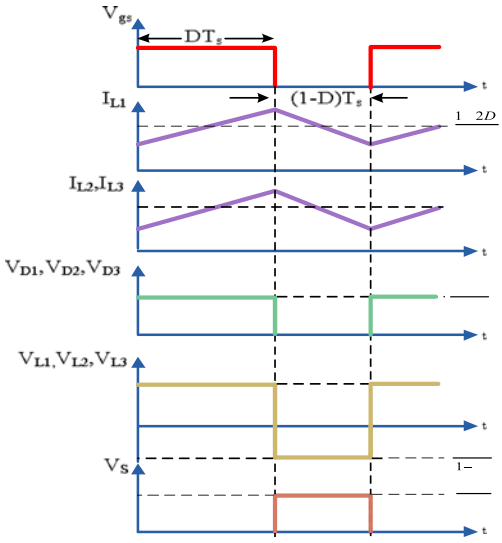

Fig. 2. Some typical waveforms of the proposed converter.

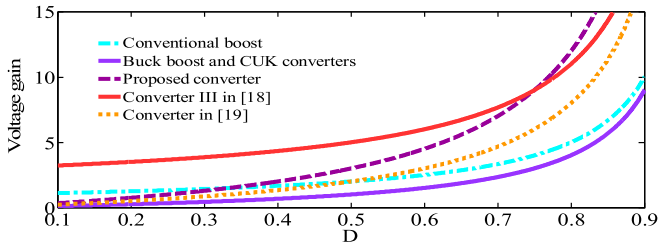

Fig. 3. Curves of voltage gain comparison of proposed converter and other converters at CCM operation.

According to (12), the voltage gain of the proposed converter is higher than that of the conventional boost, buck–boost, CUK, SEPIC, and ZETA converters and is thrice as large as the voltage gain of the conventional buck–boost converter. Fig. 2 shows some typical key waveforms of the proposed converter in CCM.

The voltage gain curves for the proposed converter, conventional boost, buck—boost, and CUK converters, proposed converter III in [18] and proposed converter in [19] are shown in Fig. 3. It is seen that the proposed converter is buck–boost and the voltage transfer gain of the converter is higher than that of the other converters.

B. Calculation of the Currents

The average current that flows through the capacitor C_o during switch ON period $(I_{\mathrm{Co,on}})$ can be achieved as follows:

$$I_{\mathrm{Co,on}} = -I_o. \tag{13}$$

The average current that flows through the capacitors C_1 and C_2 and the inductor L_2 ($I_{C1,\mathrm{on}}$, $I_{C2,\mathrm{on}}$, and I_{L2}) during switch ON period can be obtained as follows:

$$I_{C1,\mathrm{on}} = -I_{C2,\mathrm{on}} = I_{L2}. \tag{14}$$

The average current that flows through the capacitors C_3 and C_4 and the inductor L_3 during switch ON period ($I_{C3,\mathrm{on}}$, $I_{C4,\mathrm{on}}$, and I_{L3}) can be earned as follows:

$$-I_{c3,\mathrm{on}} = I_{C4,\mathrm{on}} = I_{L3}. \tag{15}$$

The average current that flows through the capacitor C_1 during switch off period $(I_{C1,\mathrm{off}})$ can be earned as follows:

$$I_{C1,\mathrm{off}} = I_{L2} - I_{C3,\mathrm{off}} - I_{L3}. \tag{16}$$

Where, $I_{C3,\mathrm{off}}$ is the average current that flows through the capacitor C_3 during switch OFF period.

The average current that flows through the capacitors C_4 $(I_{C4,\mathrm{off}})$ during switch OFF period can be achieved as follows:

$$I_{C4,\mathrm{off}} = I_{L3} - I_{Co,\mathrm{off}} - I_o \tag{17}$$

where, $I_{\mathrm{Co,off}}$ is the average current that flows through the capacitor C_o during switch OFF period.

By applying current-sec balance principle on capacitors C_1, C_2, C_3, C_4, and C_o, the following equation is derived as follows:

$$\frac{1}{T_s}\left(\int_0^{\mathrm{DT}_s} I_{C1,2,3,4,o,\mathrm{on}}\,dt + \int_{\mathrm{DT}_s}^{T_s} I_{C1,2,3,4,o,\mathrm{off}}\,dt\right) = 0 \tag{18}$$

where $I_{C2,\mathrm{off}}$ is the average current that flows through the capacitor C_2 during switch OFF period.

By substituting (13)–(17) into (18), the average current that flows through the inductors L_2 and L_3 (I_{L2} and I_{L3}) and the capacitors C_1, C_2, C_3, C_4, and C_o ($I_{C1,\mathrm{on}}$, $I_{C2,\mathrm{on}}$, $I_{C3,\mathrm{on}}$, $I_{C4,\mathrm{on}}$, and $I_{Co,\mathrm{on}}$) can be obtained as follows:

$$\begin{aligned} I_{L2} &= I_{L3} = I_{C1,\mathrm{on}} = -I_{C2,\mathrm{on}} = -I_{C3,\mathrm{on}} = I_{C4,\mathrm{on}} \\ &= -I_{Co,\mathrm{on}} = I_o. \end{aligned} \tag{19}$$

According to Fig. 1(c), the average current that flows through the inductor L_1 (I_{L1}) can be earned as follows:

$$I_{L1} = (I_{L2} + I_{C2} - I_{C1} - I_{C4})_{\mathrm{off}} = \frac{1+2D}{1-D} I_o. \tag{20}$$

According to Fig. 1(b), the average current that flows through the switch S (I_S) can be obtained as follows:

$$I_S = I_{L1} + I_{C1,\mathrm{on}} + I_{C4,\mathrm{on}} = \frac{3}{1-D} I_o. \tag{21}$$

The average of input current (I_i) can be achieved as follows:

$$I_i = \frac{1}{T_s}\left(\int_0^{\mathrm{DT}_s} (I_{L1} + I_{C1} + I_{C4})_{\mathrm{on}}\,dt\right) = \frac{3D}{1-D} I_o. \tag{22}$$

The currents that flows through the diodes D_1, D_2, and D_3 (I_{D1}, I_{D2}, and I_{D3}) can be achieved as follows:

$$I_{D1} = I_{L1} - I_{C1,\mathrm{off}} - I_{C4,\mathrm{off}} = \frac{I_o}{1-D} \tag{23}$$

$$I_{D2} = I_{L2} + I_{C1,\mathrm{off}} = \frac{I_o}{1-D} \tag{24}$$

$$I_{D3} = I_{L3} + I_{C4,\mathrm{off}} = \frac{I_o}{1-D}. \tag{25}$$

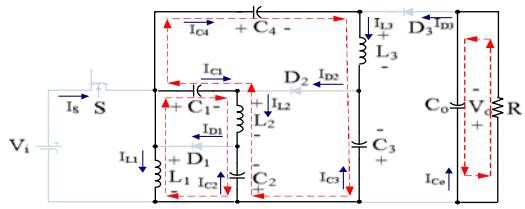

Fig. 4. Equivalent circuits of the presented converter in third mode at DCM operation.

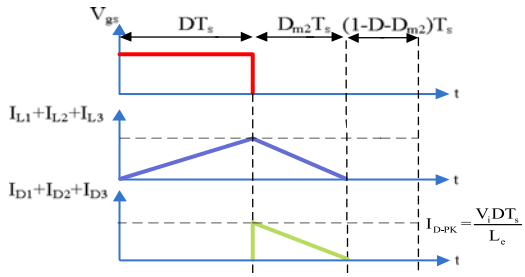

Fig. 5. Some illustrated waveforms of the proposed converter at DCM operation.

The currents ripple of inductors L_1, L_2, and L_3 $(\Delta I_{L1,2,3})$ can be calculated as follows:

$$\Delta I_{L1,2,3} = \frac{DV_i}{L_{1,2,3} f_s} = \frac{(1-D)\,V_o}{3L_{1,2,3} f_s} = \frac{V_o V_i}{(V_o + 3V_i)\,L_{1,2,3} f_s}. \tag{26}$$

C. Discontinuous Conduction Mode

The operation modes in DCM can be divided into three modes. The first mode in DCM is the same as the first mode in CCM. In the second mode, the diodes currents are decreasing and in the third mode the diodes D_1, D_2, and D_3 currents will be zero and the diodes and switch will turn OFF. The equivalent circuit and the typical waveform in third mode are shown in Figs. 4 and 5. In this mode, the inductors L_1, L_2, and L_3 currents will be constant; therefore, the voltage of the inductors L_1, L_2, and L_3 will be zero.

According to (23)–(25), the sum of the diodes D_1, D_2, and D_3 currents can be obtained as follows:

$$I_{D1} + I_{D2} + I_{D3} = I_{L1} + I_{L2} + I_{L3}. \tag{27}$$

By using (23)–(25), the average currents of diodes D_1, D_2, and D_3 $(I_{D1,\mathrm{av}}, I_{D2,\mathrm{av}}$, and $I_{D3,\mathrm{av}})$ can be achieved as follows:

$$I_{D1,\mathrm{av}} = I_{D2,\mathrm{av}} = I_{D3,\mathrm{av}} = \frac{V_o}{R}. \tag{28}$$

According to Fig. 4, the sum of the diodes D_1, D_2, and D_3 average currents during one switching period can be obtained as follows:

$$I_{D1,\mathrm{av}} + I_{D2,\mathrm{av}} + I_{D3,\mathrm{av}} = \frac{1}{2} \times D_{m2} \times I_{D-\mathrm{PK}} \tag{29}$$

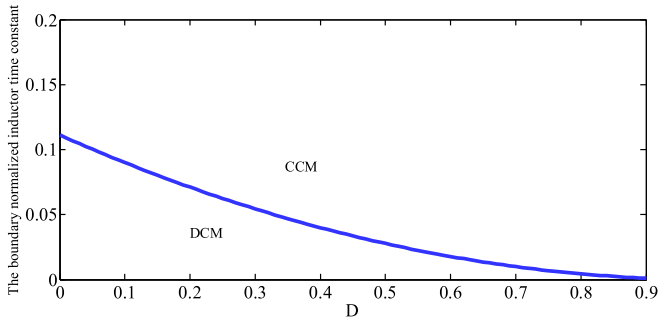

Fig. 6. Boundary normalized inductor time constant versus duty cycle.

where D_{m2} is duty cycle in second mode at DCM and $I_{\mathrm{D-PK}}$ is sum of the peak currents of inductors L_1, L_2, and L_3

$$I_{D-\mathrm{pk}} = I_{L1-\mathrm{pk}} + I_{L2-\mathrm{pk}} + I_{L3-\mathrm{pk}} = \frac{V_i D T_s}{L_{\mathrm{eq}}} \tag{30}$$

where

$$\frac{1}{L_e} = \frac{1}{L_1} + \frac{1}{L_2} + \frac{1}{L_3}. \tag{31}$$

By applying volt-sec balance principle on inductors L_1, L_2, and L_3, duty cycle in second mode at DCM (D_{m2}) can be achieved as follows:

$$D_{m2} = \frac{3DV_i}{V_o}. \tag{32}$$

By using (27)–(32), the voltage transfer gain in DCM (M_{DCM}) can be earned as follows:

$$M_{\mathrm{DCM}} = \frac{D}{\sqrt{\tau_L}} \tag{33}$$

where the parameter τ_L is expressed as follows:

$$\tau_L = \frac{2L_e}{RT_s}. \tag{34}$$

D. Boundary Condition Mode

In this mode, the voltage transfer gain of the CCM is equal to the voltage transfer gain of the DCM. According to (12) and (33), the boundary normalized inductor time constant (τ_b) can be earned as follows:

$$\tau_b = \frac{(1-D)^2}{9}. \tag{35}$$

The curve of the boundary normalized inductor time constant (τ_b) is shown in Fig. 6. If τ_L is larger than τ_b, the proposed buck–boost converter operates in CCM.

The boundary normalized inductor time constant curves for the proposed converter, proposed converter III in [18] and proposed converter in [19] are shown in Fig. 7.

E. Efficiency Analysis

For efficiency analysis of the proposed converter, parasitic resistances are defined as follows: r_{DS} is switch ON-state resistances, R_{F1}, R_{F2}, and R_{F3} are the diodes D_1, D_2, and

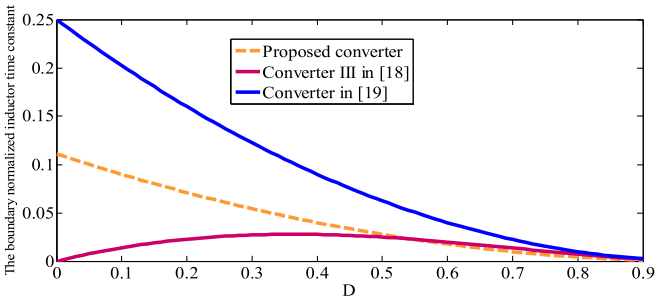

Fig. 7. Curves of boundary inductor time constant comparison of proposed converter and other converters.

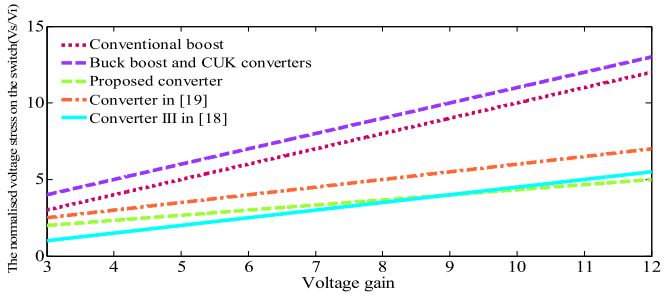

Fig. 8. Normalized switch voltage stress of the proposed converter versus voltage gain.

D_3 forward resistances, respectively, V_{F1}, V_{F2}, and V_{F3} are the diodes D_1, D_2, and D_3 threshold voltages, respectively, R_{L1}, R_{L2}, and R_{L3} are the ESR of inductors L_1, L_2, and L_3, respectively.r_{C1}, r_{C2}, r_{C3}, r_{C4}, and r_{Co} are the ESR of capacitors C_1, C_2, C_3, C_4, and C_o, respectively, and the voltage ripple across the capacitors and the inductors is ignored.

The power loss of the switch S ($P_{r\mathrm{DS}}$) can be earned as follows:

$$P_{r\mathrm{DS}} = r_{\mathrm{DS}} {I_{S,\mathrm{rms}}}^2 = r_{\mathrm{DS}} \frac{9D}{(1-D)^2} {I_o}^2. \tag{36}$$

The switching loss of the proposed converter (P_{Sw}) can be obtained as follows:

$$P_{\mathrm{Sw}} = f_s C_S {V_S}^2 = f_s C_S \left(\frac{V_i}{1-D}\right)^2. \tag{37}$$

The total losses of the switch S (P_{Switch}) can be expressed as follows:

$$P_{\mathrm{Switch}} = P_{r\mathrm{DS}} + \frac{P_{\mathrm{Sw}}}{2}. \tag{38}$$

The diodes D_1, D_2, and D_3 forward resistance losses ($(P_{\mathrm{RF}})_{D1,2,3}$) can be achieved as follows:

$$(P_{\mathrm{RF}})_{D1,2,3} = R_{F1,2,3} {I^2}_{D1,2,3,\mathrm{rms}} = R_{F1,2,3} \frac{1}{1-D} {I_o}^2. \tag{39}$$

The diodes D_1, D_2, and D_3 forward voltage losses ($(P_{\mathrm{VF}})_{D1,2,3}$) can be obtained as follows:

$$(P_{\mathrm{VF}})_{D1,2,3} = V_{F1,2,3} I_{D1,2,3,av} = V_{F1,2,3} I_o. \tag{40}$$

The power losses of capacitors C_1, C_2, C_3, C_4, and C_o ($P_{\mathrm{RC1,2,3,4,}o}$) due to them ESR, can be earned as follows:

$$\begin{aligned} P_{\mathrm{RC1,2,3,4,}o} &= r_{C1,2,3,4,o} {I_{C1,2,3,4,o,\mathrm{rms}}}^2 \\ &= r_{C1,2,3,4,o} \frac{D}{1-D} {I_o}^2. \end{aligned} \tag{41}$$

The conduction losses of inductors L_1, L_2, and L_3 (P_{rL1} and $P_{rL2,3}$) can be earned as follows:

$$P_{rL1} = R_{L1} {I^2}_{L1,\mathrm{rms}} = R_{L1} \left(\frac{1+2D}{1-D}\right)^2 {I_o}^2 \tag{42}$$

$$P_{rL2,3} = R_{L2,3} {I^2}_{L2,3,\mathrm{rms}} = R_{L2,3} {I_o}^2. \tag{43}$$

TABLE I
COMPARISON BETWEEN PROPOSED CONVERTER AND OTHER STRUCTURES

Converter in	Proposed converter	Converter in ref.	Conventional buck–boost converter
Quantities of switches	1	1	1
Quantities of diodes	3	2	1
Quantities of capacitors	5	4	1
Quantities of inductors	3	3	1
Total device count	12	10	4
Voltage stress of the switch	$\frac{V_o+3}{3}$	$\frac{V_o+2}{2}$	V_o+1
Voltage gain	$\frac{3D}{1-D}$	$\frac{2D}{1-D}$	$\frac{D}{1-D}$

The total power loss of the proposed converter (P_{Loss}) can be obtained as follows:

$$\begin{aligned} P_{\mathrm{Loss}} = {} & P_{\mathrm{Switch}} + \sum_{u=1}^{3} (P_{\mathrm{RF}})_{\mathrm{Du}} + \sum_{u=1}^{3} (P_{\mathrm{VF}})_{\mathrm{Du}} \\ & + \sum_{u=1}^{4} P_{\mathrm{RC}u} + P_{\mathrm{RC}o} + P_{rL1} + P_{rL2} + P_{rL3}. \end{aligned} \tag{44}$$

The efficiency of the proposed converter (η) can be defined as follows:

$$\eta = \frac{P_O}{P_O + P_{\mathrm{Loss}}} = \frac{1}{1 + \frac{P_{\mathrm{Loss}}}{P_O}}. \tag{45}$$

According to above equations, the efficiency of the proposed converter can be rewritten as follows:

$$\eta = \frac{1}{1 + \frac{\pi}{R(1-D)^2} + \frac{f_s C_s {V^2}_i}{2(1-D)^2 R {I^2}_o}} \tag{46}$$

where

$$\begin{aligned} \pi = {} & 9D r_{\mathrm{DS}} + (1-D)(R_{F1} + R_{F2} + R_{F3}) \\ & + \frac{(1-D)^2}{I_o}(V_{F1} + V_{F2} + V_{F3}) \\ & + D(1-D)(r_{C1} + r_{C2} + r_{C3} + r_{C4} + r_{Co}) \\ & + (1+2D)^2 R_{L1} + (1-D)^2 (R_{L2} + R_{L3}). \end{aligned} \tag{47}$$

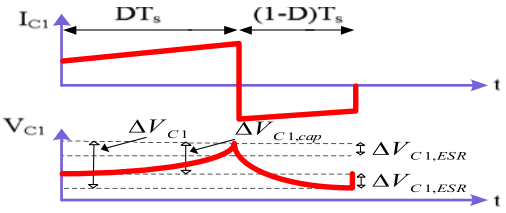

Fig. 9. Current and voltage of the capacitor C_1.

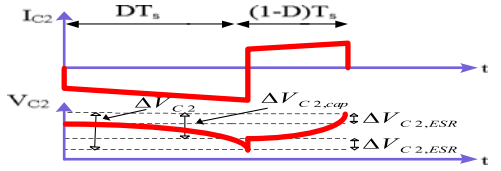

Fig. 10. Current and voltage of the capacitor C_2.

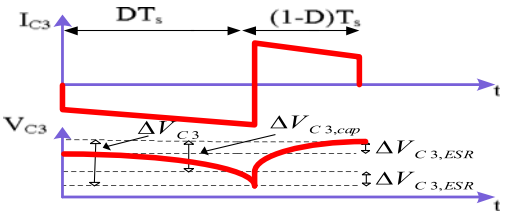

Fig. 11. Current and voltage of the capacitor C_3

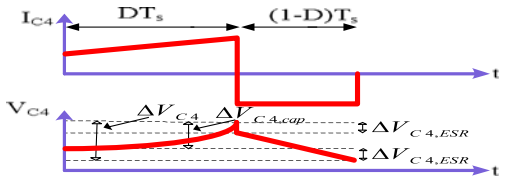

Fig. 12. Current and voltage of the capacitor C_4.

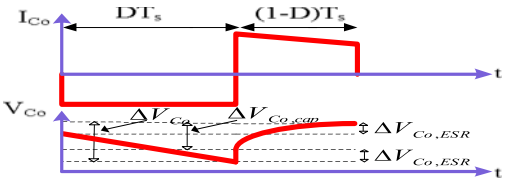

Fig. 13. Current and voltage of the capacitor C_o.

F. Voltage Stress of the Switch

In this converter, the voltage stress across the active components, such as switch and diodes, is lesser than output voltage. The voltage stress on power switch (V_S) can be achieved as follows:

$$V_S = \frac{V_i}{1-D}. \tag{48}$$

The relationship between the normalized voltage stress across power switch of the proposed converter and other converters is depicted in Fig. 8. According to Fig. 8, the normalized voltage stress of the switch in the proposed converter is lesser than that in other converters.

In order to show the total device number and voltage gain of the proposed converter, conventional buck–boost, and converter

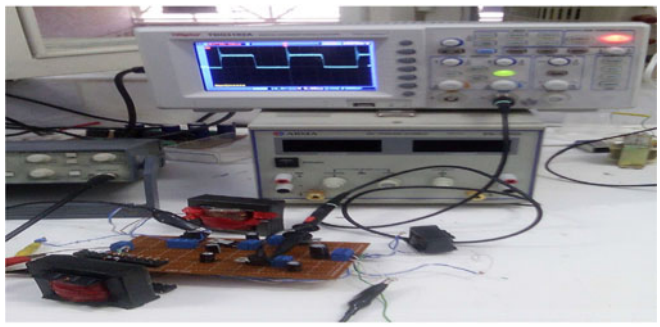

Fig. 14. Prototype of the proposed converter.

in [18], a comparison is made between the proposed topology and other converters. The device number and voltage gain of the structures are given in Table I. As shown in Table I, the proposed structure uses higher number of elements. But, the total device of the other converters is higher comparing to their gains and voltage stresses. Based on the low voltage stress of the proposed converter, the efficiency of the proposed converter is higher comparing to its gain.

G. Calculation of the Voltage Ripple of the Capacitors

From Fig. 9, the voltage ripple of the capacitor C_1 is represented by ΔV_{C1}. The voltage ripple on capacitor C_1 created from the current that flows through the ESR is signified by $\Delta V_{C1,\mathrm{ESR}}$ and the voltage ripple of capacitor C_1 created from the charging and discharging is indicated by $\Delta V_{C1,\mathrm{cap}}$.

$\Delta V_{C1,\mathrm{ESR}}$ can be calculated as follows:

$$\begin{aligned}\Delta V_{C1,\mathrm{ESR}} &= \mathrm{ESR}_{C1}\Delta I_{C1} \simeq \mathrm{ESR}_{C1}(I_{C1,\mathrm{on}} - I_{C1,\mathrm{off}}) \\ &= \frac{\mathrm{ESR}_{C1} I_o}{(1-D)}\end{aligned} \tag{49}$$

where

$$\mathrm{ESR}_{C1} = \frac{\tan\delta_{C1}}{2\pi f_s} \tag{50}$$

where, $\tan\delta_{C1}$ is the dissipation factor of capacitor C_1.

$\Delta V_{C1,\mathrm{cap}}$ can be achieved as follows:

$$\Delta V_{C1,\mathrm{cap}} = \frac{I_{C1,\mathrm{on}} DT_s}{C_1} = \frac{DT_s V_o}{RC_1}. \tag{51}$$

Hence, ΔV_{C1} can be achieved as follows:

$$\Delta V_{C1} = \Delta V_{C1,\mathrm{ESR}} + \Delta V_{C1,\mathrm{cap}} = \frac{ESR_{C1} I_o}{1-D} + \frac{DT_s V_o}{RC_1}. \tag{52}$$

Similarly, the voltage ripple of the capacitors C_2, C_3, C_4 and C_o $(\Delta V_{C2,3,4,o})$ can be achieved as follows:

$$\begin{aligned}\Delta V_{C2,3,4,o} &= \Delta V_{C2,3,4,o,\mathrm{ESR}} + \Delta V_{C2,3,4,o,\mathrm{cap}} \\ &= \frac{ESR_{C2,3,4,o} I_o}{1-D} + \frac{DT_s V_o}{RC_{2,3,4,o}}.\end{aligned} \tag{53}$$

The current and voltage of the capacitors C_2, C_3, C_4, and C_o are shown in Figs. 10—13.

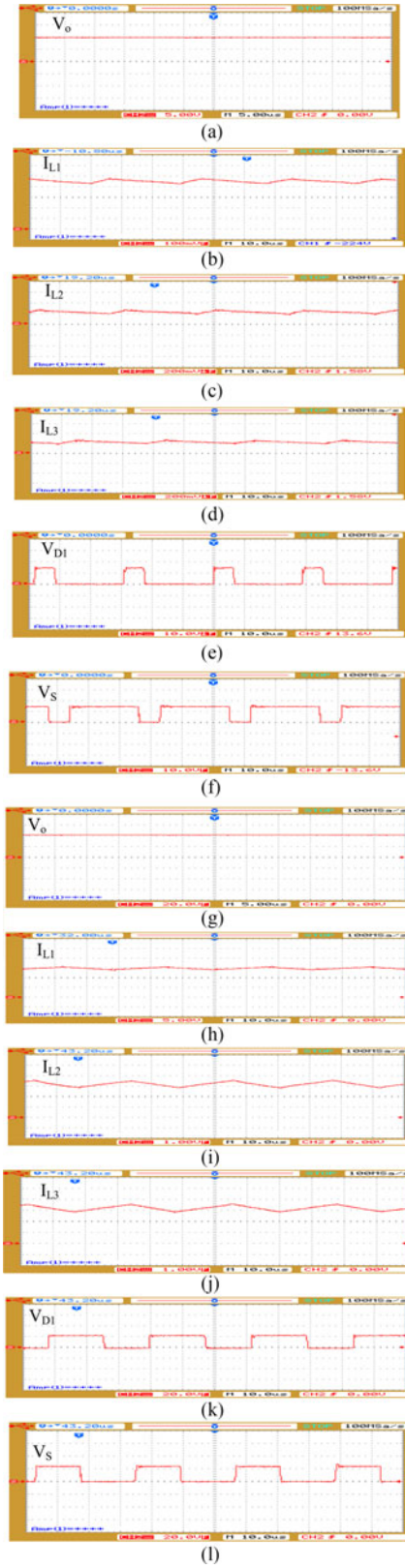

Fig. 15. Experimental results, (a) output voltage, (b) inductor L_1 current, (c) inductor L_2 current, (d) inductor L_3 current, (e) diode D_1 voltage, (f) switch S voltage, (g) output voltage, (h) inductor L_1 current, (i) inductor L_2 current, (j) inductor L_3 current, (k) diode D_1 voltage, (l) switch S voltage.

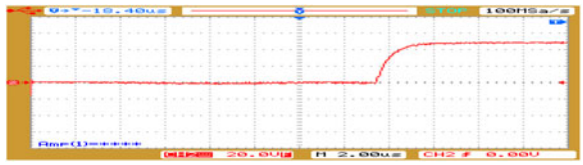

Fig. 16. Output voltage changing with ramping out.

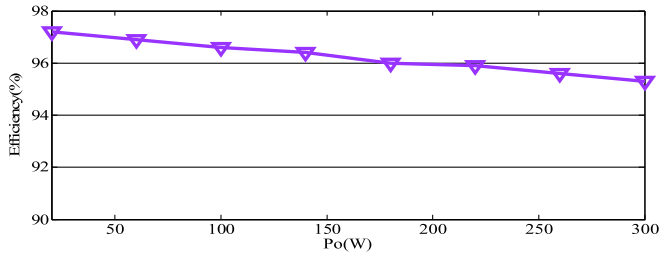

Fig. 17. Measured efficiency of the proposed converter versus output power.

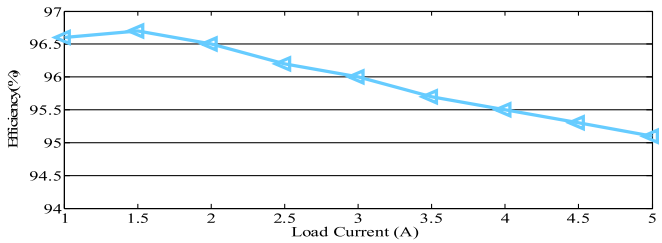

Fig. 18. Measured efficiency of the proposed converter versus load current.

IV. Experimental Results

A prototype of the proposed buck–boost converter is built as shown in Fig. 14. To demonstrate the performance of the presented converter, experimental results are provided. The proposed converter components specifications are as follows:

1) input voltage: 11 V;
2) switching frequency (buck): 37 kHz;
3) switching frequency (boost): 33 kHz;
4) switch: IRFP460A;
5) diodes D_1, D_2, and D_3: MUR860;
6) inductor L_1 (buck): 1 mH;
7) inductors L_2 and L_3 (buck): 580 μH;
8) inductor L_1 (boost): 100 μH;
9) inductors L_2 and L_3 (boost): 260 μH;
10) capacitors C_1,C_2, C_3 and C_4: 100 μF;
11) capacitor C_o: 470 μF.

The proposed converter is tested in the buck and boost states operation. The proposed converter is operated in CCM operation mode. In the buck state operation, the output voltage waveform is shown in Fig.15(a). The output voltage is equal to 10 V. The inductors L_1, L_2, and L_3 currents waveforms are shown in Fig.15(b), (c), and (d), respectively. According to (19) and (20), the average values of inductors L_1, L_2, and L_3 currents are equal to 0.45, 0.24, and 0.24 A, respectively, which closely agree with the experimental results. The voltages of diodes D_2 and D_3 waveforms are not shown since the diodes waveforms are similar to diode D_1 voltage waveform. The voltage of diode

D_1 waveform is shown in Fig.15(e). The voltage of the switch S is shown in Fig.15(f). In the boost state operation, the output voltage is shown in Fig.15(g). The output voltage is equal to 42 V and the output power is equal to 135 W. The inductors L_1, L_2, and L_3 currents waveforms are shown in Fig.15(h), (i), and (j), respectively. According to (19) and (20), the average values of inductors L_1, L_2, and L_3 currents are equal to 15.4, 3.2, and 3.2 A, respectively, which closely agree with the experimental results. The voltage of the diode D_1 is shown in Fig.15(k). The voltage across switch S is shown in Fig.15(l). Fig.16 shows the output voltage changing with ramping up. Fig.17 shows the curve of presented buck–boost converter efficiency versus output power. The maximum efficiency is appropriately 97.3%. The full-load efficiency is around 95.2%. Fig.18 shows the curves of efficiency of the proposed converter versus load current.

V. Conclusion

In this paper, a novel transformer less buck–boost dc–dc converter was presented. The structure of the presented buck–boost converter is simple. In the proposed converter, only one main switch is utilized, which decreases the conduction loss of power switch and improves efficiency. The voltage stress across the power switch is low and switch with low on-state resistance can be selected. The step-up voltage gain of the proposed buck–boost converter is higher than that of the classic boost, buck–boost, CUK, SEPIC, and ZETA converters. The proposed converter has simple structure; therefore, the control of the presented converter will be easy. The buck–boost converters is utilized in many applications like gadgets such, as mobile phones and notebooks, fuel-cell systems, car electronic devices, and LED drivers. Finally, the experimental results were provided to verify the feasibility of the proposed converter.

References

[1] K. Jin, X. Ruan, M. Yang, and M. Xu, "A hybrid fuel cell power system," *IEEE Trans. Ind. Electron.*, vol. 56, no. 4, pp. 1212–1222, Apr. 2009.

[2] W. S. Liu, J. F. Chen, T. J. Liang, R. L. Lin, and C. H. Liu, "Analysis, design, and control of bidirectional cascoded configuration for a fuel cell hybrid power system," *IEEE Trans. Power Electron.*, vol. 25, no. 6, pp. 1565–1575, Jun. 2010.

[3] S.-K. Changchien, T.-J. Liang, J.-F. Chen, and L.-S. Yang, "Novel high step-up DC-DC converter for fuel cell energy conversion system," *IEEE Trans. Ind. Electron.*, vol. 57, no. 6, pp. 2007–2017, Jun. 2010.

[4] W. Jiang and B. Fahimi, "Active current sharing and source management in fuel cell-battery hybrid power system", *IEEE Trans. Ind. Electron.*, vol. 57 , no. 2 , pp. 752–761, Feb. 2010.

[5] A. A. Ahmad and A. Abrishamifar, "A simple current mode controller for two switches buck-boost converter for fuel cells, in *Proc. IEEE Elect. Power Conf.*, 2007, pp. 363–366.

[6] R. J. Wai, C. Y. Lin, R. Y. Duan, and Y. R. Chang, "High-efficiency DC–DC converter with high voltage gain and reduced switch stress," *IEEE Trans. Ind. Electron.*, vol. 54, no. 1, pp. 354–364, Feb. 2007.

[7] T. J. Liang, J. H. Lee, S. M. Chen, J. F. Chen, and L. S. Yang, "Novel isolated high-step-up dc–dc converter with voltage lift," *IEEE Trans. Ind. Electron.*, vol. 60, no. 4, pp. 1483–1491, Apr. 2013.

[8] G. Spiazzi, P. Mattavelli, and A. Costabeber, "Effect of parasitic components in the integrated boost-flyback high step-up converter," in *Proc. 35th Annu. Conf. IEEE Ind. Electron. Soc.*, Nov. 2009, pp. 420–425.

[9] H. C. Shu, "Design and analysis of a switched-capacitor-based step-up dc/dc converter with continuous input current," *IEEE Trans. Circuits Syst. I, Fundam. Theory Appl.*, vol. 46, no. 6, pp. 722–730, Jun. 1999.

[10] Y. P. Hsieh, J. F. Chen, T. J. Liang, and L. S. Yang, "Novel high step-up DC–DC converter with coupled-inductor and switched-capacitor techniques," *IEEE Trans. Ind. Electron.*, vol. 59, no. 2, pp. 998–1007, Feb. 2012.

[11] O. Abutbul, A. Gherlitz, Y. Berkovich, and A. Ioinovici, "Step-up switching-mode converter with high voltage gain using a switched-capacitor circuit." *IEEE Trans. Circuits Syst. I*, Fundam. Theory Appl., vol. 50, no. 8, pp. 1098–1102, Aug. 2003.

[12] K. I. Hwu and W.Z. Jiang, "Isolated step-up converter based on fly-back converter and charge pumps," *IET Power Electron.*, vol. 7, no. 9, pp. 2250–2257, Sep. 2014.

[13] S. M. Chen, T. J. Liang, L. S. Yang, and J. F. Chen, "A boost converter with multiplier and coupled inductor for AC module applications," *IEEE Trans. Ind. Electron.*, vol. 60, no. 4, pp. 1503–1511, Apr. 2013.

[14] S. C. Tan *et al.*, "Switched-capacitor converter configuration with low EMI emission obtained by interleaving and its large-signal modeling," in *Proc. IEEE Int. Symp. Circuits Syst.*, May 2009, pp. 1081–1084.

[15] Y. P. Hsieh, J. F. Chen, L. S. Yang, C. Y. Wu, and W. S. Liu, "High-conversion-ratio bidirectional dc–dc converter with coupled inductor," *IEEE Trans. Ind. Electron.*, vol. 61, no. 1, pp. 210–222, Jan. 2014.

[16] T.-J. Liang and J.-H. Lee, "Novel-high-conversion-ratio high efficiency isolated bidirectional DC-DC converter," *IEEE Trans. Ind. Electron.*, vol. 62 , no. 7 , pp. 4492–4503, Jul. 2015.

[17] C. T. Pan, C. F. Chuang, and C. C. Chu, "A novel transformerless interleaved high step-down conversion ratio DC-DC converter with low switch voltage stress," *IEEE Trans. Ind. Electron.*, vol. 61 , no. 10 , pp. 5290–5299, Oct. 2014.

[18] L. S. Yang, T. J. Liang, and J. F. Chen, "Transformer-less DC–DC converter with high voltage gain," *IEEE Trans. Ind. Electron.*, vol. 56, no. 8, pp. 3144–3152, Aug. 2009.

[19] M. R. Banaei, H. Ardi, and A. Farakhor, "Analysis and implementation of a new single-switch buck–boost DC/DC converter," *IET Power Electron.*, vol. 7, no. 7, pp. 1906–1914, Jul. 2014.

[20] K. I. Hwu and T. J. Peng, "A novel buck boost converter combining KY and buck converters," *IEEE Trans. Power Electron.*, vol. 27 , no. 5, pp. 2236–2241, May 2012.

[21] A. Ajami, H. Ardi, and A. Farakhor, "Design, analysis and implementation of a buck–boost DC/DC converter," *IET Power Electron.*, vol. 7, no. 12, pp. 2902–2913, Dec. 2014.

[22] A. A. Boora, F. Zare, and A. Ghosh, "Multi-output buck-boost converter with enhanced dynamic response to load and input voltage changes," *IET Power Electron.*, vol. 4, no. 2 pp. 194–208, Feb. 2011.

[23] T.-J. Liang and J.-H. Lee, "Double-deck buck-boost converter with soft switching operation," *IEEE Trans. Power. Electron.*, vol. 31 , no. 6 , pp. 4324–4330, Jun. 2016.

[24] M. He, F. Zhang, J. Xu, P. Yang, and T. Yan, "High-efficiency two-switch tri-state buck-boost power factor correction converter with fast dynamic response and low-inductor current ripple," *IET Power Electron..*, vol. 6, no. 8, pp. 1544–1554, Sep. 2013.

Mohamad Reza Banaei was born in Tabriz, Iran. He received the M.Sc. degree in control engineering from the Polytechnic University of Tehran, Iran, in 1999, and the Ph.D. degree in power engineering from the Electrical Engineering Faculty, Tabriz University, Tabriz, Iran, in 2005.

He is a Professor in the Electrical Engineering Department, Azarbaijan Shahid Madani University, Tabriz, Iran, which he joined in 2005. His main research interests include the design and control of power electronic converters, renewable energy systems, modeling and control of FACTS, and custom power devices and power system dynamics.

Hossein Ajdar Faeghi Bonab was born in Bonab, Iran, in 1991. He received the B.S. degree in power engineering from Tabriz University, Tabriz, Iran, and the M.S. degree in power engineering from Azarbaijan Shahid Madani University, Tabriz, Iran, in 2012 and 2015, respectively.

His research interests are power electronics converters, dc–dc converters, and renewable energy.